Proceedings of ASME Turbo Expo 2023
Turbomachinery Technical Conference and Exposition
GT2023
June 26-30, 2023, Boston, Massachusetts

GT2023-103191

NUMERICAL INVESTIGATION OF NH_3 DOPED FUELS FROM BIOMASS GASIFICATION ON FUEL-BOUND NO_x FORMATION AT GAS TURBINE CONDITIONS

Silin Yang [1,*], Ahmed Raslan[1], Antoine Durocher[1,2], Felix Guethe[3], Jeffrey Bergthorson[1]

[1]Alternative Fuels Laboratory, McGill University, Montreal, Quebec, Canada
[2]Gas Turbine Laboratory, National Research Council, Ottawa, Canada
[3]Phoenix Biopower, Stockholm, Sweden

ABSTRACT

As our society transitioning away from fossil fuel-based energy system to reduce carbon emissions, renewable energy sources are needed to meet the increasing energy demand in the near future. Biomass, consisting mostly of plant-based organic materials, is a promising alternative to fossil fuels for carbon-neutral energy production. Unfortunately, during the gasification process, the nitrogen content in biomass is converted to NH_3, which is then oxidized in the combustion process, leading to high NO_x emissions through the fuel-NO pathway. The high NO_x emissions from NH_3 and NH_3-containing fuels have prevented their implementation at scale. Depending on the gasification process, source of biomass, and combustion technology, the NH_3 and water content can vary greatly. This works focuses on blends of 2% (mol) NH_3 in CH_4*, diluted by up to 55% (mass) water. The combustion process is modelled by freeflame connected to a plug flow reactor (PFR), achieving a total residence time of 100 ms. Major chemistry involved in the fuel NO pathway were identified from reaction pathway analysis. NO_x emissions were investigated under different equivalence ratios (Φ = 0.45-2.2) and inlet pressures (1 atm, 40 atm). NO concentration increases rapidly as NH_3 is added to the fuel mixture, as expected. Under fuel rich conditions, NO decreases after the initial increase, and this reduction becomes more pronounced at elevated pressure and long residence times. At the same time, unburned NH_3 and other reactive N species increase as NO decreases. The optimal conditions that minimize the total NO_x and NH_3 emissions were found to be slightly fuel rich, high pressure, and long residence time. Under these conditions, additional pathways involving NNH and N_2O promotes the conversion of NH_3 to N_2. Large discrepancies among different thermochemical mechanisms highlight areas that still need to be researched. Results from the current study can assist in the modelling and design of low-emissions engines fuelled by biomass and NH_3, thereby contributing to a carbon-neutral economy.*

Keywords: Alternative fuel, biomass, ammonia combustion, nitrogen oxides, fuel NO_x emission

NOMENCLATURE

Roman letters

BTC	Biomass-fired TopCycle
CH_3	Methyl Radical
CH_4	Methane
n_i	Mole of species i
N_2	Nitrogen
NH_3	Ammonia
NO_x	Nitrogen oxides (NO+NO_2+N_2O)
PFR	Plug flow reactor
PSR	Perfectly stirred reactor
RPA	Reaction pathway analysis
SCR	Selective catalytic reduction
S_L	Laminar burning velocity [m s^{-1}]
SNCR	Selective non-catalytic reduction
X_i	Mole fraction of species i

Greek letters

τ	Residence time [ms]
ϕ	Fuel to air equivalence Ratio
Ω	Steam to air mass ratio

1. INTRODUCTION

Combustion of fossil fuels is a major source of energy production in our society. Carbon emissions from combustion processes are significant contributors to global warming and lead to various environmental problems. With increasingly stringent regulations on pollutant emissions, renewable energy carriers are considered as potential replacements for conventional fossil fuels. Biomass provides a secure and consistent energy source and is able to complement intermittent energy sources such as

---

*Corresponding author: silin.yang@mail.mcgill.ca

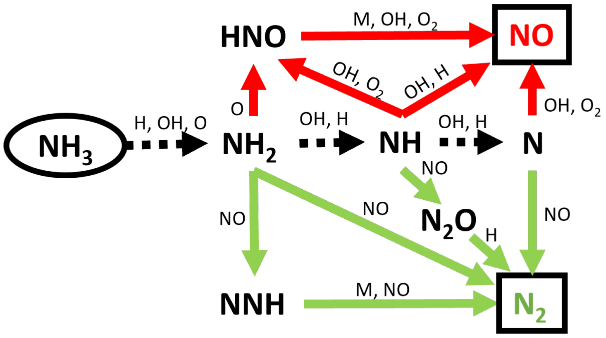

FIGURE 1: NH_3 OXIDATION PATHWAY, INCLUDING NO PRODUCTION (RED ARROW) AND REBURN (GREEN ARROW) ROUTE [2–4]

solar and wind. Numerous efforts are underway to improve the current biomass combustion processes in more sustainable and economical ways. An advanced biomass-fired TopCycle (BTC) combustion system [1] was developed by Phoenix BioPower. In the TopCycle process, biomass is gasified and combusted with air and steam at high pressure to produce energy for electricity generation. Steam injection limits the flame temperature to be under 1800 K to reduce NO_x emissions from the thermal pathway. The exhaust gas contains more than 50% (mass) steam and less than 5% (mol) NH_3. The BTC system has a large recirculation zone to allow long flames residence times (up to 100 ms) to take advantage of the NO reburn chemistry. The BTC process offers up to 60% electric power efficiency from biomass, making it twice as efficient as traditional technologies, and promising for a wide range of applications [1].

During biomass gasification, the nitrogen content in biomass converts mostly to NH_3. NH_3 is a source of fuel-bound nitrogen and can lead to high levels of NO through the fuel-NO pathway, in addition to NO production pathways via the thermal, prompt, NNH, and N_2O routes in fuels without nitrogen content. The high NO_x emissions from NH_3 have prevented the large-scale adoption of biomass-derived syngas as carbon-neutral alternatives. Depending on the operating conditions, NH_3 can either act as a key NO_x precursor in the fuel NO pathway in combustion systems, or as a reducing agent to convert NO to N_2 in the thermal DeNO$_x$ process (Figure 1). NO production, represented by red arrows in Figure 1, is driven by the presence of H/OH radicals, while NO reduction (green arrows in Figure 1) is largely determined by the available N/NH$_i$ radicals. Current thermal DeNO$_x$ methods with NH_3 (selective catalytic reduction (SCR), selective non-catalytic reduction (SNCR)) requires installation of additional units which can be expensive to build and operate. Additional in-situ combustion controls need to be investigated to reduce NO_x emissions in NH_3-containing flames while maintaining combustor operating range and efficiency.

Some studies show that NO_x emissions from NH_3 can be reduced at high pressure and fuel rich conditions. In NH_3/air flames, NO concentration increases with ϕ and peaks at slightly fuel lean condition $\phi = 0.9$ [3]. Duynslaegher et al. [5] showed numerically that increase in pressure and ϕ lead to decrease in NO emission. The decrease of NO at fuel rich conditions is accompanied by an increase in unburned NH_3 concentration [6]. Okafor et al. [7] proposed a rich-lean combustion strategy for NH_3 fuelled combustor, and identified the minimum $NO_x + NH_3$ emission occurs at $\phi = 1.1$ and ambient pressure of 0.3 MPa. Similarly, in laminar stagnation flames, slightly rich equivalence ratio of $\phi = 1.06$ was found to reduce both NO_x and unburned NH_3 in the product gas [8]. They also reported that NO_x emissions in NH_3-air flames consist mostly of NO. At elevated pressures, increased sensitivity of reactions $OH + H + M \leftrightarrow H_2O + M$ and $H + O_2 + M \leftrightarrow HO_2 + M$ depletes the available H/OH radicals to oxidize NH$_i$ radicals into NO through HNO [7, 9, 10]. The excess NH_3 at richer conditions promote NO reduction reactions by NH$_i$ [8, 9, 11]

Contrary to CH_4 combustion, NH_3 combustion requires a long residence time for NO oxidation to complete. Wang et al. [12] studied the effect of residence time in premixed swirl flames by altering the combustion chamber length and the swirl number, and reported that increasing swirl number is more effective than increasing chamber length in reducing NO_x. Another study reported that NO reduction in NH_3/H_2/air flames at long residence time is caused by the excess NH$_i$ radical pool consuming NO [13]. Due to the abundance of NO and N atoms, the reaction $N_2 + O \leftrightarrow NO + N$ is favoured in the backward direction in NH_3/H_2/air flames as opposed to CH_4/air flames [13]. Only lean equivalence ratios of $0.5 \leqslant \phi \leqslant 0.95$ were investigated in [12, 13], it is unclear whether the reducing effect of long residence time also applies to fuel rich conditions.

Water dilution has been suggested as a promising NO_x reduction approach in NH_3 combustion. [14–17]. Pugh et al. [14] studied premixed swirling NH_3/H_2/air flames, and showed that reactant humidification limits thermal NO pathway, and promotes NO reburn in the post flame through increased OH/NH_2 interaction. Since water leads to higher concentrations of unburnt NH_3, fuel lean operation is preferable for humidified combustion in order to offset the unburnt fuel fractions [14]. Similarly, Bozo et al. [15] showed that steam injection reduces NO_x by lowering flame temperature and suppressing break down of NH_3. Steam injection of around 40% (mass) in 70%NH_3/30%H_2 (mol) swirl stabilized flames achieve stable flames with efficiencies comparable to humidified natural gas cycles [15].

Addition of CH_4 to NH_3 opens up additional NH_3 oxidation pathways through CH_3 [2]. The combined effects of NH_3/CH_4 chemistry contribute to the uncertainty in NO_x modelling predictions, especially under fuel rich conditions [2]. A review on adding H_2 and CH_4 to NH_3-based combustion by Chai et al. [18] explains that NH_3 and CH_4 oxidation occurs in parallel, sharing the same H/OH radical pool. Han et al. [19] compared S_L measurements in NH_3/CH_4 premixed flames with 3 kinetic mechanisms, and showed that modeling results deviate the most from the measured data under rich conditions and at higher χ_{CH_4} in the fuel blend. The source of the discrepancy lies in the N-containing reactions, and C-N interactions have little impact on S_L and the flame structure [19]. Even small amounts of NH_3, relevant to the application of TopCycle, could significantly increase NO_x emissions. Sullivan et al. [20] investigated that only 1000 ppm of NH_3 addition to CH_4 diffusion flames increases NO emission from 25 ppm to 297 ppm. Jojka et al. [21] showed that doubling

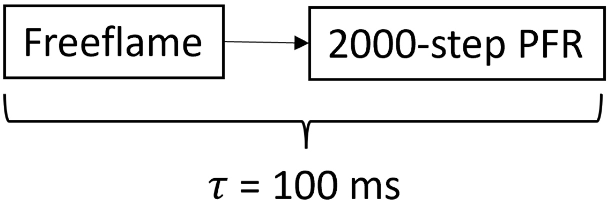

FIGURE 2: SCHEMATIC OF THE MODELLING NETWORK

of NH_3 concentration from 2.5% to 5% (mol) in CH_4 premixed flames increases flue gas NO emission by about 50%.

Understanding how NH_3 interacts with CH_4 is crucial in the study of fuel NO oxidation chemistry, and is necessary for the modelling and design of low-emissions engines fuelled by biomass and NH_3. The purpose of this paper is to numerically investigate the fuel NO pathway in water diluted CH_4 flames with 2% (mol) NH_3 addition at engine relevant conditions. A parametric study varying equivalence ratio and residence time is conducted to identify the optimal condition for minimizing NO_x formation at engine conditions. The fuel NO chemistry at the optimal condition is then studied using reaction pathway analysis and sensitivity analysis to understand the major NO production and consumption pathways. Predictions from 3 thermochemical mechanisms are also compared to assess the differences in fuel NO production at the optimal condition.

2. METHODOLOGY

In this study, the combustion process is modelled by a 1D freely propagating flame connected to a 0D PFR in Cantera [22] (Figure 2), a similar simulation setup is reported previously in [23]. The main reaction zone is modelled by a 1D freely propagating flame, which is simulated using Cantera's freeflame model with multicomponent transport and energy equation enabled. The starting grid refinement criteria for ratio, slope, and curve are 2, 0.5, and 0.9, respectively. The slope and curve are adaptively refined to ~ 0.007 (slope) and ~ 0.01 (curve) to obtain solutions with at least 500 gridpoints and 1 μm grid size. The beginning of flame, $\tau = 0$, is defined as the point of maximum heat release in the freeflame simulation. The residence time of main reaction zone is dependant on the domain length and flame speed in the freeflame simulation, varying between 1-2 ms for different equivalence ratios. Information on the product gas composition, pressure and temperature at the end of the freeflame simulation is then fed into the post flame zone. A 0D plug flow reactor (PFR) containing 2000 perfectly stirred reactors (PSRs) is used to simulate the heat release in the post flame region.

The global reaction of NH_3/CH_4 mixture with air under stoichiometric condition is given by:

$$X_{NH_3}NH_3 + \left(1 - X_{NH_3}\right) CH_4 + \left(2 - \frac{5}{4}X_{NH_3}\right) (O_2 + 3.76N_2) \tag{1}$$

$$\rightarrow \left(1 - X_{NH_3}\right) CO_2 + \left(2 - \frac{X_{NH_3}}{2}\right) H_2O + \left(7.52 - 4.2X_{NH_3}\right) N_2 \tag{2}$$

TABLE 1: SUMMARY OF SIMULATION CONDITIONS

T_{ad} (K)	T_{in} (K)	P_{in} (atm)	ϕ	Ω (mass)	X_{NH_3} (mol)
1800	773.15	1,40	0.5-2.2	0-55%	2 %

where X_{NH_3} is the molar fraction of NH_3 with respect to the fuel mixture, defined as:

$$X_{NH_3} = \frac{n_{NH_3}}{n_{NH_3} + n_{CH_4}} \tag{3}$$

When the flame is not stoichiometric, the amount of the fuel becomes $\phi[X_{NH_3}NH_3 + (1 - X_{NH_3})\, CH_4]$.

Steam is added to the mixture at different dilution levels to maintain a constant adiabatic temperature of 1800K. The steam content is defined as the steam-to-air mass ratio:

$$\Omega = \frac{\dot{m}_{\text{steam}}}{\dot{m}_{\text{air}}} \tag{4}$$

The simulation conditions (Table 1) are selected based on the operating conditions of the TopCycle process, in which the inlet temperature is around 773.15K, inlet pressure around 40 atm, combustor temperature around 1800K, and X_{NH_3} around 2% (mol). Since the BTC system has a large recirculation zone, the residence time is simulated up to 100 ms. A wide sweep of equivalence ratios ($\phi = 0.5$ - 2.2) and a long residence time is used to study the NO production and reburn chemistry over different equivalence ratios and time.

NO simulations from 3 mechanisms are compared: Okafor mechanism [24], Glarborg mechanism [2] with the updated NH_3 chemistry [25], and Wang [26] mechanism. The Okafor mechanism is designed based on the chemistry of the GRI mechanism [27] for natural gas combustion, with additional NH_3 oxidation chemistry. It contains 59 species and 356 reactions, and has been compared with experimental ignition delay time and laminar burning velocity data in NH_3/air [19], NH_3/H_2 [28], NH_3/CH_4 [3, 29] and NH_3/syngas blends [30]. Glarborg et al. [2] reviewed the thermochemistry data for key nitrogen species and the rate parameters for gas-phase nitrogen reactions in the combustion of light hydrocarbons (mostly CH_4) and light fuel-nitrogen species (NH_3, HCN and HNCO). The NH_3 sub-mechanism in [2] was recently updated based on batch reactor and flow reactor results in the NH_3/NO_2 system [25]. The updated mechanism contains 153 species and 1412 reactions. The Wang mechanism [26] is developed based on the ELTE mechanism by Varga et al. [31] for H_2 and syngas combustion, with additional NH_3 sub-mechanism collected from a NH_3/syngas mechanism by Han et al. [30], as well as C-N interaction reactions taken from San Diego mechanism [32] and Konnov mechanism [33, 34] for light hydrocarbon combustion. It contains 91 species and 444 reactions and has been validated for experimental laminar flame velocity data in NH_3/H_2, NH_3/CH_4, NH_3/CH_3OH, and NH_3/C_2H_5OH blends [26].

The NO_x emission index is used to quantify and compare the potential NO_x produced in CH_4/NH_3/air flames. The NO_x emission index is defined as the sum of all reactive N species other than N_2:

$$\text{NO Emission Index} = \sum_{i=1}^{n} n_i X_{N_i} \tag{5}$$

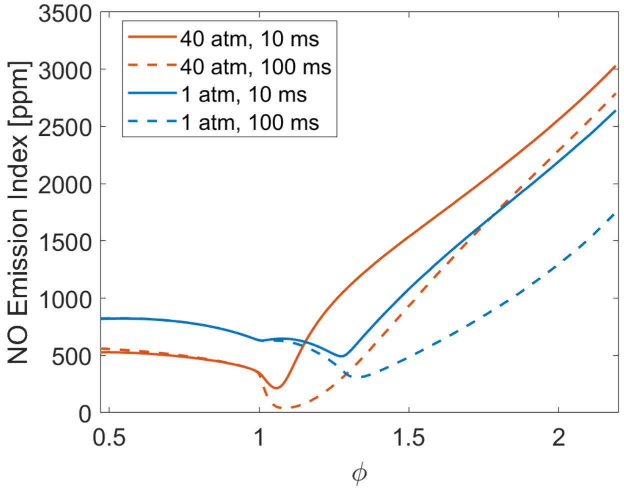

FIGURE 3: NO EMISSION INDEX WITH RESPECT TO ϕ, OKAFOR MECHANISM

where X_{N_i} is the molar concentration of reactive N species N_i, and n_i is the moles of NO that can be oxidized from 1 mole of species N_i (e.g. $NNH + O_2 \rightarrow 2NO + H$, $n_{NNH} = 2$). This NO_x emission index accounts for all reactive N species that are potentially harmful, including NO_x and unburnt NH_3 in the product gas. N_2 is the only N species that is unaccounted for in the NO_x emission index, this means that the lower the NO_x emission index, the more initial nitrogen (either from N_2 or fuel bound nitrogen) is converted to N_2 that doesn't contribute to harmful N emission. Comparison of NO index under different conditions provides insight into the optimal region for minimizing total N emissions.

3. RESULTS AND DISCUSSION

3.1 NO_x emission index for gas turbine condition

Figure 3 shows the changes in NO emission index subjected to 3 different parameters: equivalence ratio ϕ, residence time τ and inlet pressure P_{in}, simulated using the Okafor mechanism. With increase in ϕ, the NO emission index decreases first then increases at fuel rich condition. Elevated pressure reduce NO emission index for lean to slightly rich equivalence ratios compared to atmospheric pressure. For P_{in} = 40 atm, the minimum NO emission index occurs at slightly rich condition, $\phi = 1.06$ at τ = 10 ms and $\phi = 1.08$ at τ = 100 ms. For P_{in} = 1 atm, the minimum equivalence ratio shifts to richer condition $\phi = 1.28$ at τ = 10 ms and $\phi = 1.32$ at τ = 100 ms. For both pressures at fuel rich conditions, the NO emission index drops with increasing residence time.

The main species that contribute to the total NO emission index are shown in Figure 4. NO and NH_3 are inversely correlated: NO is the dominant N species at fuel lean conditions, and NH_3 is the dominant species at fuel rich conditions. The minimum NO emission index occurs at the equivalence ratio where the most NH_3 is converted to N_2 without excess NH_3 emitted. In order to understand the changes near the 'valley' in Figure 4, the rest of this section will focus on understanding the changes in NO_x chemistry near the 'valley' in Figure 4, right before and after the minimum NO_x emission at $\phi = 1.06$, and comparing NO predictions among different mechanisms at this optimal condition to identify key differences in NO promoting/reburn pathways.

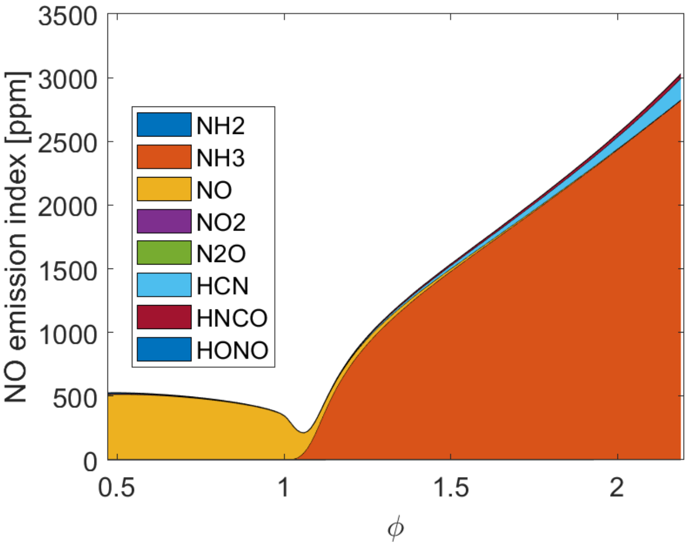

FIGURE 4: NO EMISSION INDEX WITH RESPECT TO ϕ AT 10 MS, P_{in} = 40 ATM, OKAFOR MECHANISM

3.2 NO production at P_{in} = 40 atm

It was shown from Figure 3 that at P_{in} = 40 atm, the optimal condition for minimizing total NO_x emission is around slightly fuel rich $\phi = 1.06$. This minimum condition, along with a fuel lean condition $\phi = 0.8$, and a richer condition at $\phi = 1.2$, are selected for further analysis of NO chemistry. Figure 5a and Figure 5b show the NO and NH_3 profiles with respect to residence time for the selected 3 equivalence ratios, simulated using the Okafor mechanism. At $\phi = 0.8$, NO increases rapidly at flame front then increases slowly post flame. At $\phi = 1.06$ and 1.2, NO is produced rapidly at the flame front, reaching a maximum at around 0.5 ms after the maximum heat release, then decreases with time.

As seen in Figure 5a, the maximum NO obtained at fuel rich conditions are much lower than fuel lean conditions. One reason is the amount of initial NH_3 that are reacted to form NO or N_2. Figure 5c presents the conversion of initial NH_3 to NO/N_2/unburned NH_3 at $\tau = 0.5$ ms, based on Okafor mechanism simulation. For fuel rich conditions, a significant portion of NH_3 remains unreacted post flame, resulting in less NH_3 available to be oxidized to NO. For $\phi = 0.8$, all of the initial NH_3 is used up in the flame front, whereas $\sim 18\%$ (mol) and $\sim 73\%$ (mol) of the initial NH_3 remains unburnt at 0.5 ms after maximum heat release for $\phi = 1.06$ and $\phi = 1.2$, respectively. Figure 6 presents the brute force sensitivity results for NH_3 concentrations at $\tau = 0.5$ ms, simulated using the Okafor mechanism. X_{NH_3} sensitivity is calculated based on Equation 6 below, where dk is the amount of the perturbation on the individual reaction rates, set to 1%. Both the forward and reverse directions are affected by the perturbation. A positive X_{NH_3} sensitivity suggests that X_{NH_3} increases when the perturbed

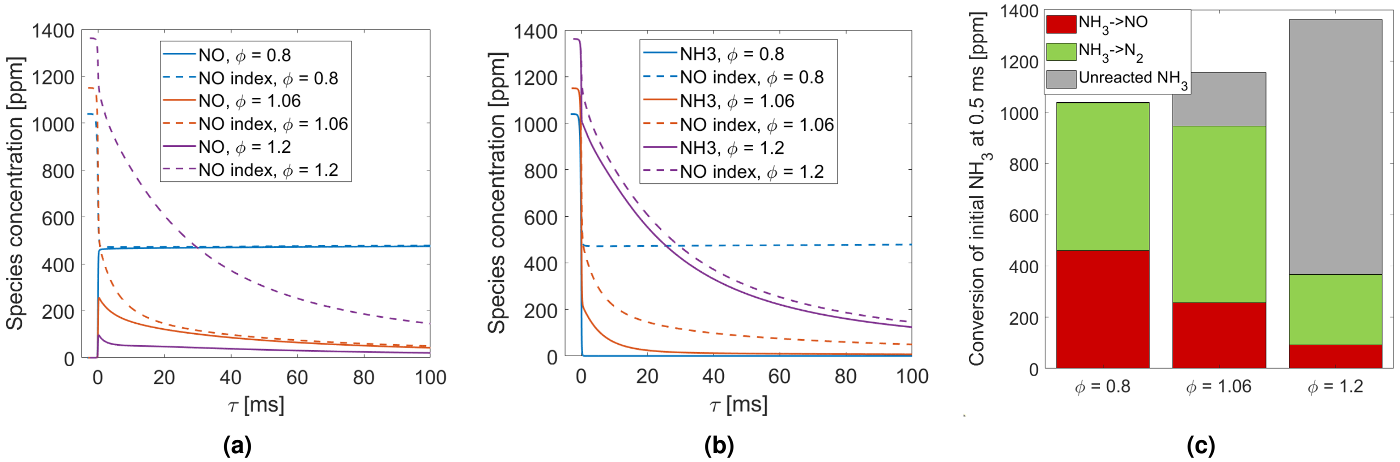

FIGURE 5: PROFILES OF A) NO AND NO INDEX VS τ, B) NH_3 AND NO INDEX VS τ, AND C) CONVERSION OF INITIAL NH_3 TO NO/N_2 AT τ = 0.5 MS FOR ϕ = 0.8, 1.06 AND 1.2

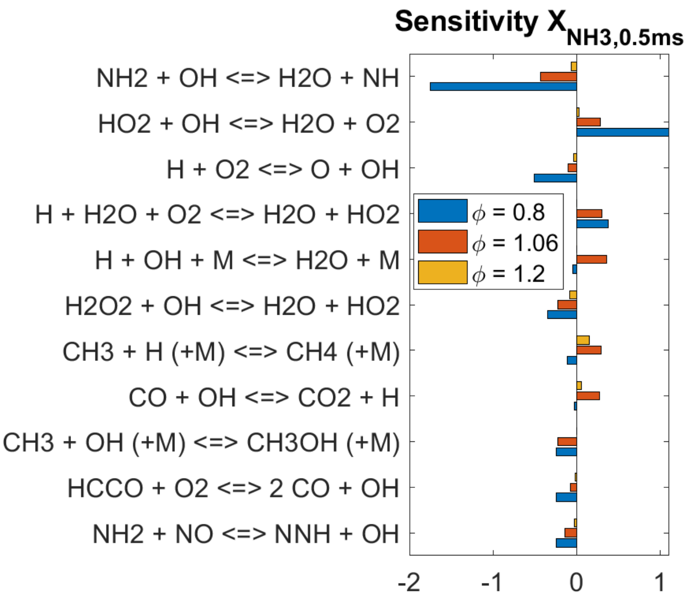

FIGURE 6: SENSITIVITY ANALYSIS FOR X_{NH_3} AT τ = 0.5 MS , OKAFOR MECHANISM

reaction proceed in the forward direction.

$$\text{Sensitivity } X_{NH_3,0.5ms} = \frac{X_{NH_3,0.5ms,perturbed} - X_{NH_3,0.5ms,base}}{X_{NH_3,0.5ms,base} \times dk} \tag{6}$$

X_{NH_3} is heavily dependant on the OH radical pool. Reaction $NH_2 + OH \rightarrow H_2O + NH$ has a strong negative X_{NH_3} sensitivity at $\phi = 0.8$, indicating the influence of OH radicals in consuming NH_3 under fuel lean conditions. Other highly X_{NH_3} sensitive reactions at $\phi = 0.8$ either produce OH ($H + O_2 \rightarrow O + OH$) or consume OH ($HO_2 + OH \rightarrow H_2O + O_2$). The lack of OH radicals at fuel rich conditions impede the break down of NH_3 at the flame front for further oxidation.

Additionally, the amount of reacted NH_3 conversion to N_2 decreases as the fuel/air mixture becomes richer. From Figure 5c, ∼ 44% (mol) of reacted NH_3 emit as NO for the lean condition $\phi = 0.8$, however this conversion reduces to 28% (mol) for fuel rich conditions $\phi = 1.06$ and $\phi = 1.2$. In order to understand the NO production routes for different equivalence ratios, reaction pathway analysis (RPA) of the nitrogen atom is computed at the maximum NO emission around $\tau = 0.5$ ms using the Okafor mechanism (Figure 7). The thickness of the arrows in the RPA corresponds to the net flux of reactive N species integrated over the computation domain (in this case, from the start of the simulation to $\tau = 0.5$ ms). Only fluxes greater than 5% of the total outflux are shown in the RPA for clarity. The color on the fluxes represents the sensitivity of each path to NO concentration at $\tau = 0.5$ ms.

In the combustion of NH_3/CH_4 mixture with air, NO can be produced from NH_3 (fuel-bound nitrogen) and N_2 in the air. The RPAs in Figure 7 show a net influx of NH_3 and a net outflux of N_2 and NO crossing the control volume from start to 0.5 ms residence time. Even with only 2% NH_3 (mol) present in the fuel mixture, fuel-NO production is dominant over other NO pathways that originate from N_2. For all equivalence ratios, the reacted NH_3 converts into either NO or N_2. The main $NH_3 \rightarrow NO$ production

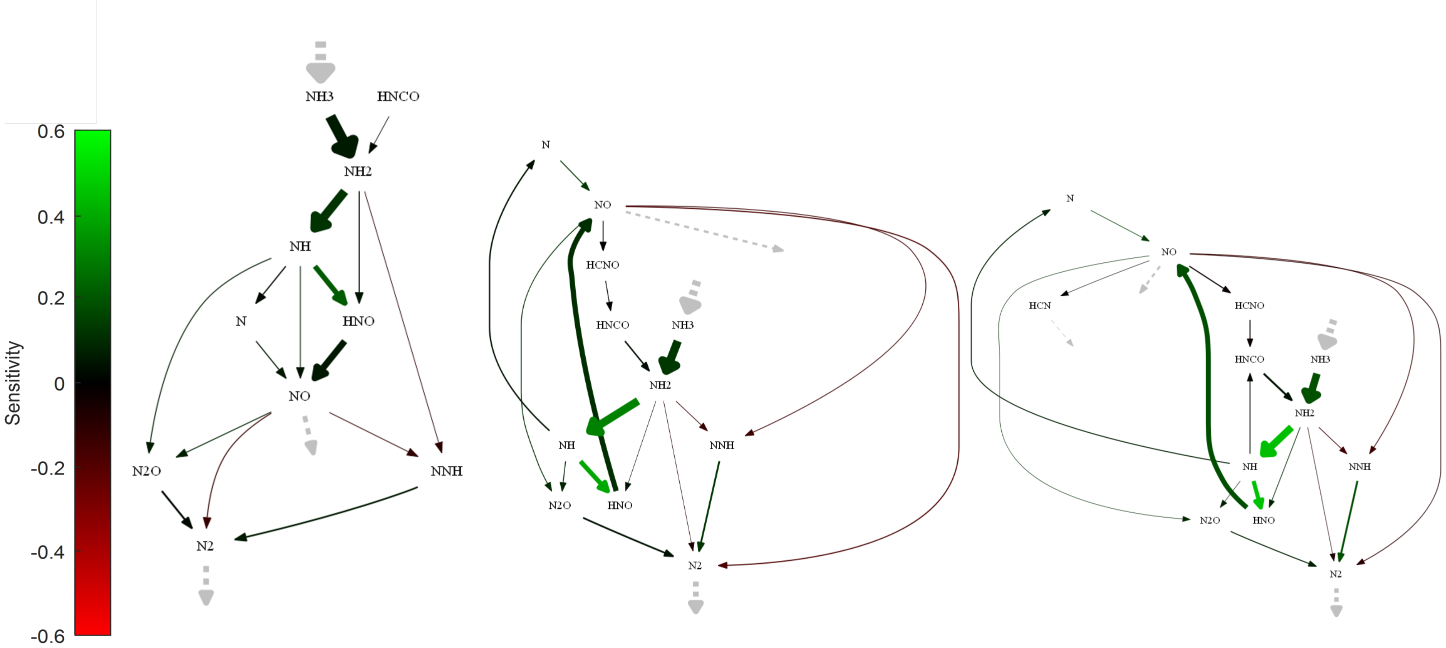

(a) ϕ **= 0.8** **(b)** ϕ **= 1.06** **(c)** ϕ **= 1.2**

FIGURE 7: RPA TRACKING FLUXES OF NITROGEN ATOMS BETWEEN START OF SIMULATION TO τ = 0.5 MS, THE DASHED GREY ARROWS REPRESENTS THE INFLUX AND OUTFLUX OF N SPECIES CROSSING THE RPA CONTROL VOLUME, THE OTHER ARROWS ARE COLORED BASED ON BRUTE FORCE NO SENSITIVITY RESULTS AT τ = 0.5 MS (FIGURE 8), OKAFOR MECHANISM

route is through HNO:

$$NH_3 \xrightarrow{OH} NH_2 \xrightarrow{OH,H} NH \xrightarrow{CO_2,OH,O_2} HNO \xrightarrow{H,OH,O_2} NO \tag{7}$$

Other routes through NH and N, namely $NH + O_2 \rightarrow NO + OH$ and $N + O_2 \rightarrow NO + O$, also play a minor role in NO formation. The main $NH_3 \rightarrow N_2$ route is through NNH and N_2O, which are mostly formed from reactions of NH and NH_2 radicals with NO:

$$NH \xrightarrow{NO} N_2O \xrightarrow{O,OH,H,M} N_2 \tag{8}$$

$$NH_2 \xrightarrow{NO} NNH \xrightarrow{H,OH,O_2} N_2 \tag{9}$$

Although similar $NH_3 \rightarrow N_2/NO$ routes are present for fuel lean and fuel rich conditions, the contribution of individual reactions can vary. Figure 8 compares the sensitivity of NO concentrations to individual reaction rates at $\tau = 0.5$ ms for the Okafor mechanism. A positive X_{NO} sensitivity means X_{NO} increases when the perturbed reaction proceed in the forward direction. Reactions that exhibit positive sensitivities for X_{NO}, e.g. $CO + HO_2 \rightarrow CO_2 + OH$, $CO_2 + NH \rightarrow CO + HNO$ and $NH_2 + OH/H \rightarrow NH + H_2O/H_2$, are important reactions involved in the HNO pathway (Equation 7), proceeding in the forward direction to promote NO production. As ϕ increases, X_{NO} sensitivities for these reactions increases, suggesting increased demand for H/OH radicals. Meanwhile, reactions involving CH_3 and O/OH, e.g. $CH_3 + H(+M) \rightarrow CH_4(+M)$ and $CH_3 + HO_2 \rightarrow CH_3O + OH$), show strong negative X_{NO} sensitivities at fuel rich conditions. These CH_3 reactions compete with NO promoting reactions such as $H + NH_2 \rightarrow H_2 + NH$ for

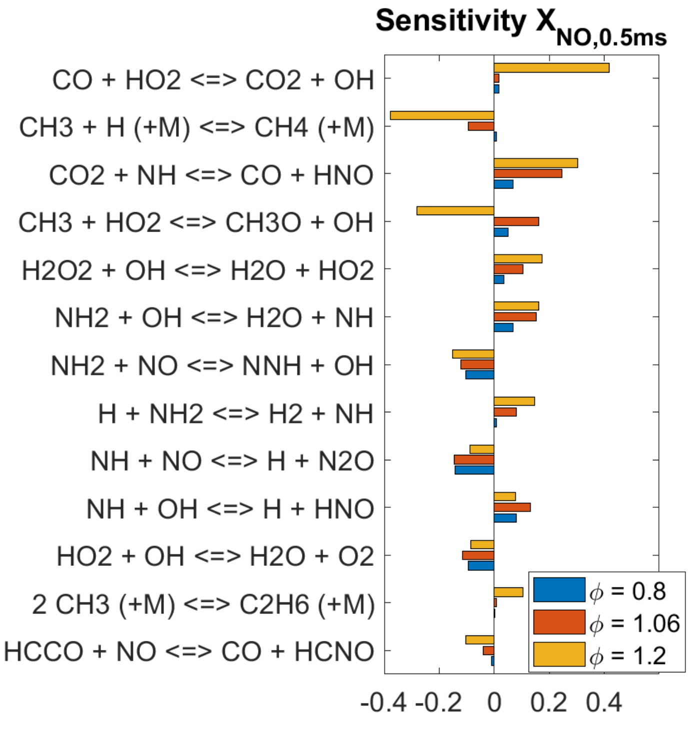

FIGURE 8: SENSITIVITY ANALYSIS FOR X_{NO} AT τ = 0.5 MS , OKAFOR MECHANISM

the H/OH radicals, hindering NO production through the HNO pathway (Equation 7) most notably for $\phi = 1.2$.

Reactions that have negative sensitivities for X_{NO}, $NH + NO \longrightarrow H + N_2O$ and $NH_2 + NO \longrightarrow NNH + OH$, take part in the N_2O (Equation 8) and NNH (Equation 9) pathway for NO reburn. Some of the NO produced recirculate back to NH_2 via HNCO:

$$NO \xrightarrow{HCCO} HNCO \xrightarrow{H} NH_2 \qquad (10)$$

The X_{NO} sensitivities for the NO reaction with HCCO, $HCCO + NO \longrightarrow CO + HCNO$, increase with richer equivalence ratios. This increased X_{NO} sensitivity suggest that more NO recirculate back to NH_2 at fuel rich conditions via HCNO, reducing the total amount of NO emitted from NH_3.

Based on the discussions above, even for <5% of NH_3 in the fuel mixture, fuel-NO production from NH_3 dominates over other NO pathways from N_2. Three factors are responsible for the decreased flame front NO production at fuel rich condition: 1) reduction of reacted NH_3 due to the lack of OH radicals; 2) reduced conversion of reacted $NH_3 \longrightarrow NO$ due to the competition between CH_3 and NO promoting reactions for H/OH radicals; 3) increased NO recirculation back to NH_2 through HNCO.

3.3 NO reburn at P_{in} = 40 atm

As noted previously in Figure 5a, after the initial sharp peak, NO concentrations drop post flame for fuel rich conditions. This decrease of X_{NO} post flame coincides with the observation in Figure 3, where NO emission index reduces with increased residence time. Figure 9 shows the RPA for the flux of N species from the time of peak X_{NO} at about 0.5 ms to 20 ms post flame for Okafor mechanism. The key difference between the RPAs in fuel lean condition (Figure 9a) and fuel rich conditions (Figure 9b and 9c), is the break down of NH_2.

At $\phi = 0.8$, NH_2 predominantly reacts with OH to form NH, producing NO through the HNO pathway (Equation 7), as well as a small contribution of thermal NO:

$$NH \xrightarrow{OH,H} N \xrightarrow{O_2,OH} NO \qquad (11)$$

One of the HNO → NO reactions produces HONO: $HNO + NO_2 \longrightarrow HONO + NO$. HONO further contributes to NO production by reacting with NH and NH_2:

$$HONO \xrightarrow{NH,NH_2} NO_2 \xrightarrow{OH,H} NO \qquad (12)$$

Figure 10 represents brute force sensitivity analysis for the change of X_{NO} between the perturbed and base equations:

$$\frac{[X_{NO,20ms} - X_{NO,0.5ms}]_{perturbed} - [X_{NO,20ms} - X_{NO,0.5ms}]_{base}}{[X_{NO,20ms} - X_{NO,0.5ms}]_{base} \times dk} \qquad (13)$$

From Figure 10, the reaction between isomers HNCO and HCNO: $H + HCNO \longrightarrow H + HNCO$ have a significant influence on the NO production post flame as HNCO react to form NH_2 in the presence of OH/H radicals. Due to the lack of NH_3 post flame, a majority of NH_2 is produced from HNCO: $HNCO + OH \longrightarrow CO_2 + NH_2$. Some of the NO produced in the flame front also react with HCCO to form HCNO: $HCCO + NO \longrightarrow CO + HCNO$, before recycling back into NO via NH_2. Under this fuel lean condition, NO competes with O_2 for available HCCO, $HCCO + O_2 \longrightarrow 2CO + OH$, which in turn affects the amount of $HCNO \longrightarrow NH_2$ conversion.

Other reactions sensitive to changes of X_{NO} between the flame front and post flame involves HO_2: $CH_3 + HO_2 \longrightarrow CH_3O + OH$, $H + H_2O + O_2 \longrightarrow H_2O + HO_2$. As shown in the sensitivity analysis of X_{NH_3} at $\tau = 0.5$ ms in Figure 6, HO_2 impacts the consumption of NH_3 in the flame front, as it competes with NH_2 for OH radicals through the reaction $HO_2 + OH \longrightarrow H_2O + O_2$. In addition, HO_2 reacts with NO to form NO_2, facilitating the HONO → NO pathway as shown in Equation 12. The role of HO_2 in converting NO to NO_2 and promoting OH radical for fuel ignition is noted in [35]. The large sensitivity of HO_2 reactions at $\phi = 0.8$ implies that HO_2 is a limiting species in the break down of $NH_3 \rightarrow NH_2 \rightarrow NO$, as well as in the NO recycle pathway $\xrightarrow{HO_2} HONO \rightarrow NO$. From Figure 10, it is also interesting to note that reaction $H_2O_2 + OH \longrightarrow H_2O + HO_2$ exhibits positive sensitivity with increasingly equivalence ratio, whereas reaction $H + H_2O + O_2 \longrightarrow H_2O + HO_2$ shows strongest X_{NO} sensitivity at the fuel lean conditions. Both reactions produce HO_2 in the forward direction and show positive X_{NO} sensitivity, but require different radical pool: H and O_2 for fuel lean condition, and OH radicals for fuel rich conditions.

At $\phi = 1.06$ and 1.2, NH_2 conversion to NH is limited by the lack of OH radicals, so a significant portion of NH_2 reacts with NO, resulting in the net NO consumption as evidenced in the RPA. Compared to the RPA in the flame front in Figure 7, NO reburn routes via NNH (Equation 9) and $NH_2 + NO \longrightarrow H_2O + N_2$ becomes dominant with more NO present post flame. In addition, CH_3 reaction with H becomes more sensitive to changes in X_{NO} under fuel rich conditions, as opposed to CH_3 reaction with HO_2 under fuel lean conditions. This reaction consumes H radicals which are key species in NO production at fuel rich conditions. At $\phi = 1.2$, some of the CH_3 also plays a role in NO recircuation to NH_2: $CH_3 + NO \longrightarrow H_2O + HCN$, producing HCN which are further converted to NH_2 via HNCO as shown in Figure 9c. With richer fuel air mixtures, more CH_3 is available in the post flame region to produce HCN, which is evidenced by the increased HCN concentration shown in Figure 4.

To sum up, in the post flame region, NH_2 breaks down via different routes to favor NO production for fuel lean condition, and NO reduction for fuel rich condition. At fuel lean conditions, most of the NH_2 break down into NH and produces NO via HNO, and the NO produced in the flame front is recycled back to NH_2 via HNCO in the presence of OH/H/HO_2. The lack of NH_3 post flame limits the NO reduction reactions between NH_i and NO. With increasing ϕ, the lack of OH radicals favors NH_2 reactions with NO. NO reburn path through NNH and NH_2 becomes dominant, resulting in a net NO reduction.

3.4 Comparing different mechanisms at P_{in} = 40 atm, ϕ = 1.06

A comparison of NO profiles of 3 mechanisms at P_{in} = 40 atm, $\phi = 1.06$ is shown in Figure 11. Similar profiles of NO production in the flame front followed by a NO reburn post flame, can be seen in all 3 mechanisms; yet their predictions of maximum

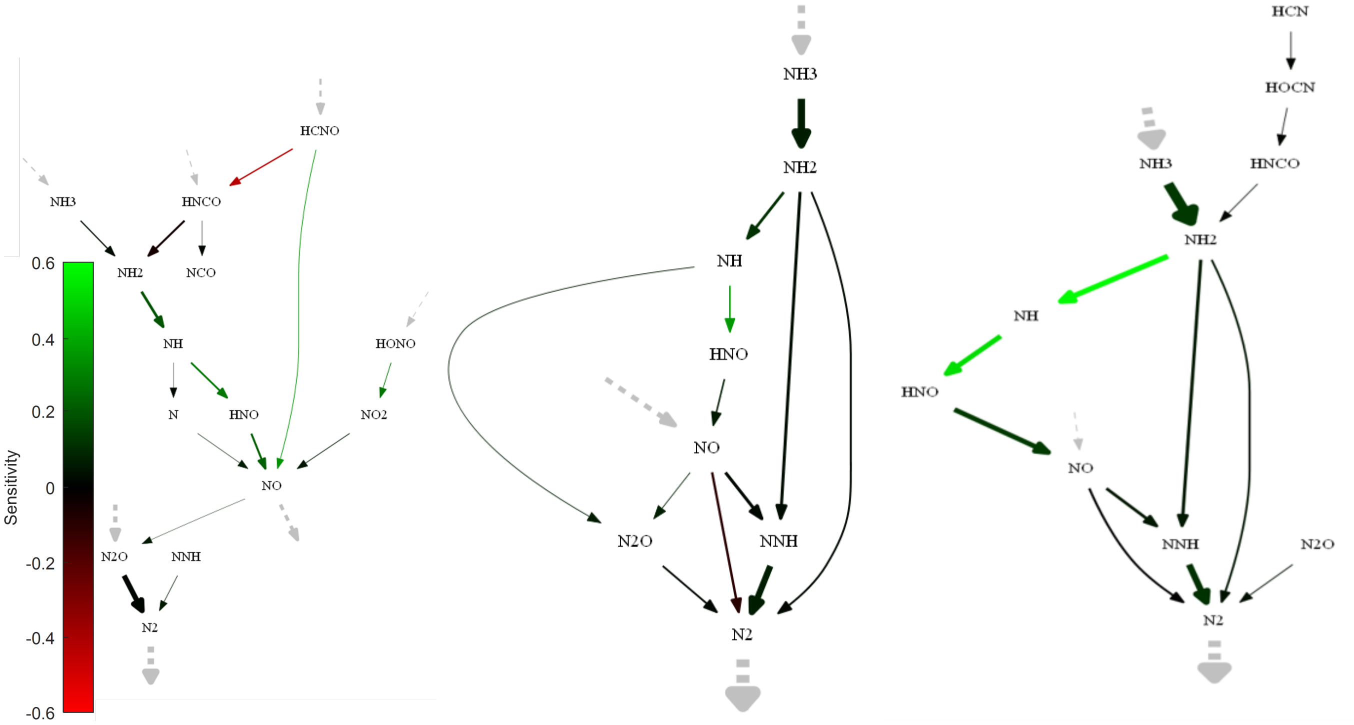

(a) ϕ = 0.8 (b) ϕ = 1.06 (c) ϕ = 1.2

FIGURE 9: RPA TRACKING FLUXES OF NITROGEN ATOMS BETWEEN τ = 0.5-20 MS, THE DASHED GREY ARROWS REPRESENTS THE INFLUX AND OUTFLUX OF N SPECIES CROSSING THE RPA CONTROL VOLUME, THE OTHER ARROWS ARE COLORED BASED ON BRUTE FORCE NO SENSITIVITY RESULTS BETWEEN τ = 0.5-20 MS (FIGURE 10), OKAFOR MECHANISM

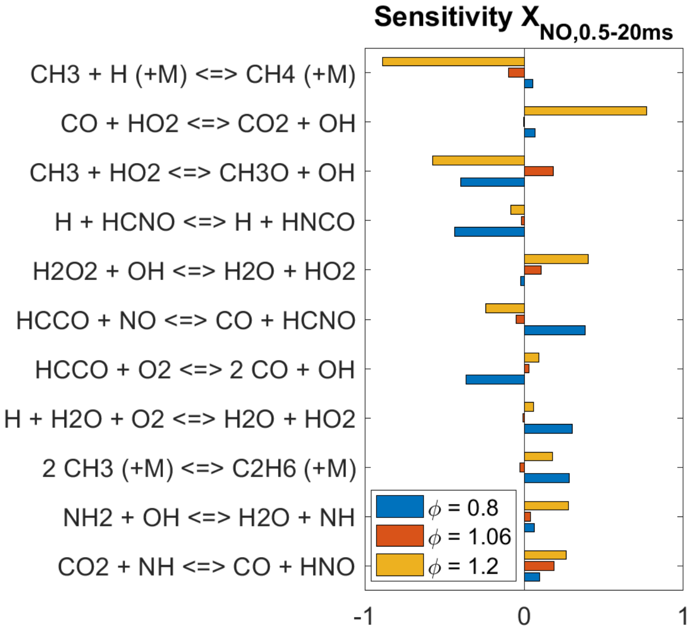

FIGURE 10: SENSITIVITY ANALYSIS FOR X_{NO} BETWEEM τ = 0.5-20 MS , OKAFOR MECHANISM

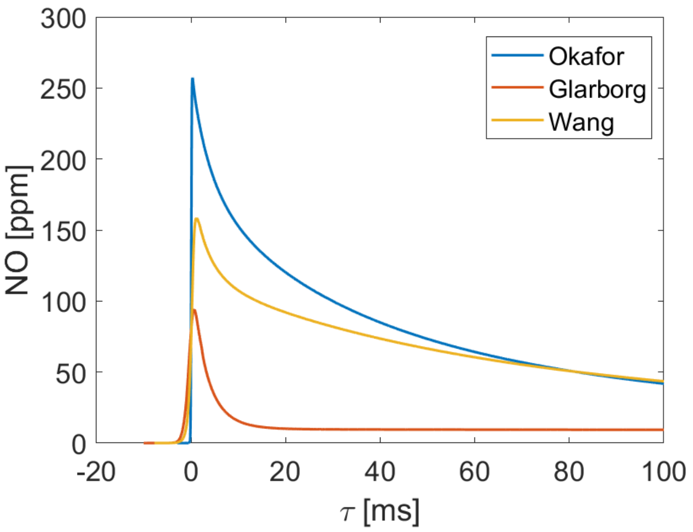

FIGURE 11: COMPARISON OF NO VS τ FOR OKAFOR, GLARBORG, AND WANG MECHANISMS

NO value vary significantly. In particular, Okafor predicts a maximum X_{NO} of ~257 ppm, while the Wang mechanism predicts a maximum X_{NO} of ~94 ppm, a 163 ppm difference under the same conditions. As mentioned in Section 2, these 3 mechanisms have been validated against shock tube or laminar flame measurements in NH_3 or NH_3/CH_4 blends, but their detailed $NH_3 \rightarrow NO$ chemistry might be different in 2 ways: 1) different reactions in the $NH_3 \rightarrow NO$ pathway, and 2) different reaction rates for the same set of $NH_3 \rightarrow NO$ reactions.

To better understand the sources of the discrepancy, sensitivity analysis for Okafor, Glarborg, and Wang mechanisms are computed at τ = 0-0.5 ms (Figure 12). Log form Arrhenius rate constants, log(K), for these X_{NO} sensitive reactions at T = 1800 K are also calculated based on the rate parameters A, b, E, provided in each mechanism:

$$\log(\mathrm{K}[\mathrm{cm}^3\mathrm{mol}^{-1}\mathrm{s}^{-1}]) = \log(\mathrm{AT}^{\mathrm{b}}\exp(\frac{\mathrm{E}}{\mathrm{RT}})) \qquad (14)$$

Table 2 summarizes the list of reactions with $\Delta\log(K) > 0.3$, which translates into maximum reaction rate K difference of factor 2 among the 3 mechanisms. Reactions involving HO_2: $HO_2 + OH \longleftrightarrow H_2O + O_2$, $H_2O_2 + OH \longleftrightarrow H_2O + HO_2$, and $CH_3 + HO_2 \longleftrightarrow CH_3O + OH$ have the highest rate discrepancy: reaction rates K differ by up to 2.8, 40, and 8.6 times, respectively.

Previous reactors studies [25, 36] show that reactions involving HO_2 and H_2NO are both important and uncertain for NH_3 oxidation. Discrepancies in these HO_2 reaction rates not only influence the H/OH radical pool for fuel breakdown, but also NO production via the HNO path. Reaction $HO_2 + NH_2 \longrightarrow H_2NO + OH$ present in Glarborg and Wang initiates an additional NO production route via H_2NO: $NH_2 \longrightarrow H_2NO \longrightarrow HNO \longrightarrow NO$. The consumption of HO_2 by OH/CH_3 species limits the $NH_2 \xrightarrow{HO_2} NO$ path, which might explain that the Glarborg and Wang predict lower amount of maximum NO than Okafor.

Reactions in the $NH \longrightarrow HNO \longrightarrow NO$ path is another source of discrepancy among the mechanisms. NH reaction with CO_2 is not present in Glarborg, potentially contributing to its lowest NO prediction. Another reaction in the same path, $NH + O_2 \longleftrightarrow HNO + O$, differ in reaction rates by a factor of 2 (Table 2).

Based on the above discussion, the discrepancies from the 3 mechanisms stem from a combination of both different reaction rates and different reactions present in the NO production routes. Reaction rates in HO_2 reactions vary by up to a factor of 40, these reactions contribute to the H/OH radical formation and NO production route via H_2NO. Mechanisms also disagree on which reactions are responsible for NO production: NH reaction with CO_2, and NH_2 reaction with H_2NO are important NO promoting reactions in some mechanisms, but not present in others. Changing the reaction rates, or adding the missing reactions might reconcile the differences for individual conditions, but won't necessarily resolve the discrepancies across a large parameter space where other routes of NO chemistry become dominant. The comparison of different mechanisms suggest that fundamental NO measurements for NH_3 is needed to validate and optimize multiple reactions in current mechanisms simultaneously.

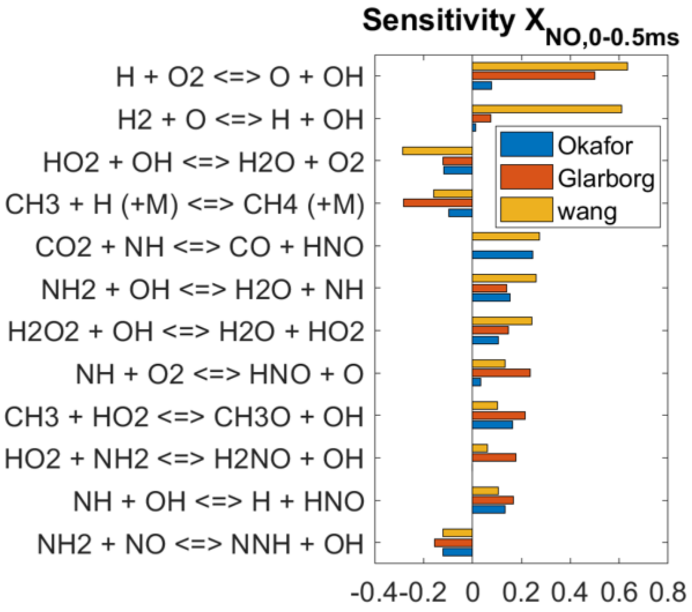

FIGURE 12: SENSITIVITY ANALYSIS FOR X_{NO} AT τ = 0-0.5 MS, OKAFOR, GLARBORG, AND WANG MECHANISMS

TABLE 2: ARRHENIUS RATE CONSTANTS FOR KEY X_{NO} SENSITIVE REACTIONS AT T = 1800 K, UNITS IN $\log(\mathrm{K}[\mathrm{cm}^3\mathrm{mol}^{-1}\mathrm{s}^{-1}])$

Reaction	Okafor	Glarborg	Wang
$HO_2 + OH \longleftrightarrow H_2O + O_2$	13.75	13.30	13.46
$H_2O_2 + OH \longleftrightarrow H_2O + HO_2$	14.66	13.06	13.06
$NH + O_2 \longleftrightarrow HNO + O$	11.38	11.7	11.7
$CH_3 + HO_2 \longleftrightarrow CH_3O + OH$	13.58	12.96	12.70

4. CONCLUSION

In conclusion, the present study investigated the fuel NO pathway in 2% (mol) NH_3/CH_4/air flames with water dilution. Numerical simulation is performed using the Cantera freeflame simulation followed by a PFR to achieve a total flame residence time of 100 ms. Results show that reduced NO emission index can be obtained at slightly rich condition at elevated pressures (P_{in} = 40 atm, ϕ = 1.06) and at long residence times. The minimum NO emission index occurs when the maximum amount of reacted NH_3 is converted to N_2. Even for only 2% NH_3, NO production and reburn from NH_3 (fuel-NO pathway) are the most dominant routes contributing to NO emission. NO is rapidly formed in the flame front mostly through the $NH_i \rightarrow HNO \rightarrow NO$ route, which is dominant at fuel lean condition due to break down of NH_3. In the post flame region, the NO reburn routes, $NH_2 + NO \rightarrow NNH + OH$ and $NH_2 + NO \rightarrow H_2O + N_2$, become dominant at fuel rich conditions due to abundance of NH_i post flame from unreacted NH_3. Mechanisms vary greatly in terms of NO predictions, and discrepancies stem from varying rates in H_2O reactions, and different reactions adopted in the $NH_3 \rightarrow NO$ production path. The numerical results from the current study will guide the design of fundamental NO measurements in NH_3 flames to assess and improve the fuel-NO chemistry of different mechanisms. A more accurate fuel-NO model can assist in the design of low-emissions engines fuelled by biomass and NH_3. Findings in the paper regarding the chemical interactions of $NH_3 \rightarrow NO/N_2$ suggest that the conventional operating strategies for minimizing NO_x emission in CH_4 flames (lean burn, short residence time) can't be applied to NH_3/CH_4 flames, and could provide insights into the design shift that is necessary for NH_3 combustion systems where fuel-NO chemistry is dominant.

ACKNOWLEDGMENTS

The author would like to acknowledge the contribution of Phoenix Biopower and financial support from the New Frontiers in Research Fund - Global 2020, EUCanWin project, and Natural Sciences and Engineering Research Council of Canada (NSERC).

REFERENCES

[1] Biopower, Phoenix. "The BTC Technology." https://phoenixbiopower.com/projects.

[2] Glarborg, P., Miller, J., Ruscic, B. and Klippenstein, S. "Modeling nitrogen chemistry in combustion." *Progress in Energy and Combustion Science* Vol. 67 (2018): pp. 31–68.

[3] Kobayashi, H., Hayakawa, A., Somarathne, K. and Okafor, E. "Science and technology of ammonia combustion." *Proceedings of the Combustion Institute* Vol. 37 No. 1 (2019): pp. 109–133.

[4] Miller, J., Smooke, M., Green, R. and Kee, R. "Kinetic modeling of the oxidation of ammonia in flames." *Combustion Science and Technology* Vol. 34 No. 1-6 (1983): pp. 149–176.

[5] Duynslaegher, C., Jeanmart, H. and Vandooren, J. "Ammonia combustion at elevated pressure and temperature conditions." *Fuel* Vol. 89 No. 11 (2010): pp. 3540–3545.

[6] Hayakawa, A., Arakawa, Y., Mimoto, R., Somarathne, K. A, Kudo, T. and Kobayashi, H. "Experimental investigation of stabilization and emission characteristics of ammonia/air premixed flames in a swirl combustor." *International Journal of Hydrogen Energy* Vol. 42 No. 19 (2017): pp. 14010–14018.

[7] Okafor, E., Somarathne, K., Hayakawa, A., Kudo, T., Kurata, O., Iki, N. and Kobayashi, H. "Towards the development of an efficient low-NOx ammonia combustor for a micro gas turbine." *Proceedings of the combustion institute* Vol. 37 No. 4 (2019): pp. 4597–4606.

[8] Hayakawa, A., Hirano, Y., Okafor, E., Yamashita, H., Kudo, T. and Kobayashi, H. "Experimental and numerical study of product gas characteristics of ammonia/air premixed laminar flames stabilized in a stagnation flow." *Proceedings of the Combustion Institute* Vol. 38 No. 2 (2021): pp. 2409–2417.

[9] Hayakawa, A., Goto, T., Mimoto, R., Kudo, T. and Kobayashi, H. "NO formation/reduction mechanisms of ammonia/air premixed flames at various equivalence ratios and pressures." *Mechanical Engineering Journal* (2015): pp. 14–00402.

[10] Somarathne, K., Hatakeyama, S., Hayakawa, A. and Kobayashi, H. "Numerical study of a low emission gas turbine like combustor for turbulent ammonia/air premixed swirl flames with a secondary air injection at high pressure." *International Journal of Hydrogen Energy* Vol. 42 No. 44 (2017): pp. 27388–27399.

[11] Meng, X., Zhao, C., Cui, Z., Zhang, X., Zhang, M., Tian, J., Long, W. and Bi, M. "Understanding of combustion characteristics and NO generation process with pure ammonia in the pre-chamber jet-induced ignition system." *Fuel* Vol. 331 (2023): p. 125743.

[12] Wang, G., Guiberti, T., Cardona, S., Jimenez, C. and Roberts, W. "Effects of residence time on the NO_x emissions of premixed ammonia-methane-air swirling flames at elevated pressure." *Proceedings of the Combustion Institute* (2022).

[13] Wang, S., Elbaz, A., Arab, O. and Roberts, W. "Turbulent flame speed measurement of NH_3/H_2/air and CH_4/air flames and a numerical case study of NO emission in a constant volume combustion chamber (CVCC)." *Fuel* Vol. 332 (2023): p. 126152.

[14] Pugh, D., Bowen, P., Valera-Medina, A., Giles, A., Runyon, J. and Marsh, R. "Influence of steam addition and elevated ambient conditions on NOx reduction in a staged premixed swirling NH_3/H_2 flame." *Proceedings of the combustion institute* Vol. 37 No. 4 (2019): pp. 5401–5409.

[15] Božo, M., Vigueras-Zuniga, M., Buffi, M., Seljak, T. and Valera-Medina, A. "Fuel rich ammonia-hydrogen injection for humidified gas turbines." *Applied energy* Vol. 251 (2019): p. 113334.

[16] Okafor, E., Somarathne, K., Ratthanan, R., Hayakawa, A., Kudo, T., Kurata, O., Iki, N., Tsujimura, T., Furutani, H. and Kobayashi, H. "Control of NO_x and other emissions in micro gas turbine combustors fuelled with mixtures of methane and ammonia." *Combustion and flame* Vol. 211 (2020): pp. 406–416.

[17] Chiong, M., Chong, C., Ng, J., Mashruk, S., Chong, W., Samiran, N., Mong, G. and Valera-Medina, A. "Advancements of combustion technologies in the ammonia-fuelled engines." *Energy Conversion and Management* Vol. 244 (2021): p. 114460.

[18] Chai, W., Bao, Y., Jin, P., Tang, G. and Zhou, L. "A review on ammonia, ammonia-hydrogen and ammonia-methane fuels." *Renewable and Sustainable Energy Reviews* Vol. 147 (2021): p. 111254.

[19] Han, X., Wang, Z., Costa, M., Sun, Z., He, Y. and Cen, K. "Experimental and kinetic modeling study of laminar burning velocities of NH_3/air, NH_3/H_2/air, NH_3/CO/air and NH_3/CH_4/air premixed flames." *Combustion and Flame* Vol. 206 (2019): pp. 214–226.

[20] Sullivan, N., Jensen, A., Glarborg, P., Day, M., Grcar, J., Bell, J., Pope, C. and Kee, R. "Ammonia conversion and NOx formation in laminar coflowing nonpremixed methane-air flames." *Combustion and Flame* Vol. 131 No. 3 (2002): pp. 285–298.

[21] Jojka, J. and Ślefarski, R. "Dimensionally reduced modeling of nitric oxide formation for premixed methane-air flames with ammonia content." *Fuel* Vol. 217 (2018): pp. 98–105.

[22] Goodwin, D., Speth, R., Moffat, H. and Weber, B. "Cantera: an object-oriented software toolkit for chemical kinetics, thermodynamics, and transport Processes." https://www.cantera.org (2021). DOI 10.5281/zenodo.4527812. Version 2.5.1.

[23] Dybe, S., Bluemner, R., Zhang, K., Schimek, S., Duwig, C., Stathopoulos, P., Paschereit, C. O. and Bartlett, M. "Design and Experimental Characterization of a Swirl-Stabilized Combustor for Low Calorific Value Gaseous Fuels." *Journal of Engineering for Gas Turbines and Power* Vol. 144 No. 2 (2022).

[24] Okafor, E., Naito, Y., Colson, S., Ichikawa, A., Kudo, T., Hayakawa, A. and Kobayashi, H. "Measurement and modelling of the laminar burning velocity of methane-ammonia-air flames at high pressures using a reduced reaction mechanism." *Combustion and Flame* Vol. 204 (2019): pp. 162–175.

[25] Glarborg, P. "The NH_3/NO_2/O_2 system: Constraining key steps in ammonia ignition and N_2O formation." *Combustion and Flame* (2022): p. 112311.

[26] Wang, Z., Han, X., He, Y., Zhu, R., Zhu, Y., Zhou, Z. and Cen, K. "Experimental and kinetic study on the laminar burning velocities of NH_3 mixing with CH_3OH and C_2H_5OH in premixed flames." *Combustion and Flame* Vol. 229 (2021): p. 111392.

[27] Smith, G., Golden, D., Frenklach, M., Moriarty, N., B., Goldenberg, M., Bowman, C., Hanson, R., Song, S., Jr., W. Gardiner, Lissianski, V. and Qin, Z. "GRI-Mech 3.0." http://combustion.berkeley.edu/gri-mech.

[28] da Rocha, R., Costa, M. and Bai, X. "Chemical kinetic modelling of ammonia/hydrogen/air ignition, premixed flame propagation and NO emission." *Fuel* Vol. 246 (2019): pp. 24–33.

[29] Okafor, E., Naito, Y., Colson, S., Ichikawa, A., Kudo, T., Hayakawa, A. and Kobayashi, H. "Experimental and numerical study of the laminar burning velocity of CH_4-NH_3-air premixed flames." *Combustion and flame* Vol. 187 (2018): pp. 185–198.

[30] Han, X., Wang, Z., He, Y., Zhu, Y. and Cen, K. "Experimental and kinetic modeling study of laminar burning velocities of NH_3/syngas/air premixed flames." *Combustion and Flame* Vol. 213 (2020): pp. 1–13.

[31] Varga, T, Olm, C., Nagy, T., Zsély, I., Valkó, É., Pálvölgyi, R., Curran, H. and Turányi, T. "Development of a joint hydrogen and syngas combustion mechanism based on an optimization approach." *International journal of chemical kinetics* Vol. 48 No. 8 (2016): pp. 407–422.

[32] Mechanical and Aerospace Engineering (Combustion Research), University of California at San Diego. "Chemical-Kinetic Mechanisms for Combustion Applications." http://web.eng.ucsd.edu/mae/groups/combustion/mechanism.html. San Diego Mechanism web page.

[33] Konnov, A. "Implementation of the NCN pathway of prompt-NO formation in the detailed reaction mechanism." *Combustion and Flame* Vol. 156 No. 11 (2009): pp. 2093–2105.

[34] Han, X., Marco, L., Brackmann, C., Wang, Z., He, Y. and Konnov, A. "Experimental and kinetic modeling study of NO formation in premixed CH_4+O_2+N_2 flames." *Combustion and Flame* Vol. 223 (2021): pp. 349–360.

[35] Gokulakrishnan, P., Shao, J., Klassen, M., Davidson, D. and Hanson, R. "NO_x formation from ammonia, and its effects on oxy-combustion of hydrocarbon fuels under supercritical-CO_2 conditions." *Applications in Energy and Combustion Science* Vol. 13 (2023): p. 100110.

[36] Cornell, R., Barbet, M., Lee, J. and Burke, M. "NH_3 oxidation by NO_2 in a jet-stirred reactor: The effect of significant uncertainties in H_2NO kinetics." *Applications in Energy and Combustion Science* Vol. 12 (2022): p. 100095.